Atmospheric
Chemistry
and Physics
Discussions

Open Access

EGU

Influence of temperature on the molecular composition of ions

and charged clusters during pure biogenic nucleation

Carla Frege[1], Ismael K. Ortega[2], Matti P. Rissanen[3], Arnaud P. Praplan[3], Gerhard Steiner[3,4,5],

Martin Heinritzi[6], Lauri Ahonen[3], António Amorim[7], Anne-Kathrin Bernhammer[4], Federico

Bianchi[1,3], Sophia Brilke[4], Martin Breitenlechner[4], Lubna Dada[3], António Dias[7], Jonathan

Duplissy[3,8], Sebastian Ehrhart[8], Imad El-Haddad[1], Lukas Fischer[4], Claudia Fuchs[1], Olga

Garmash[3], Marc Gonin[9], Armin Hansel[4], Christopher R. Hoyle[1], Tuija Jokinen[3], Heikki

Junninen[3], Jasper Kirkby[6,8], Andreas Kürten[6], Katrianne Lehtipalo[1,3], Markus Leiminger[6],

Roy Lee Mauldin[3,16], Ugo Molteni[1], Leonid Nichman[10], Tuukka Petäjä[3], Nina Sarnela[3],

Siegfried Schobesberger[3], Mario Simon[6], Mikko Sipilä[3], Dominik Stolzenburg[5], António

Tomé[11], Alexander L. Vogel[1,8], Andrea Wagner[6], Robert Wagner[3], Mao Xiao[1], Chao Yan[3],

Penglin Ye[12,15], Joachim Curtius[4], Neil M. Donahue[12], Rick C. Flagan[13], Markku Kulmala[3],

Douglas R. Worsnop[3,14,15], Paul M. Winkler[5], Josef Dommen[1] and Urs Baltensperger[1]

[1] Paul Scherrer Institute, Laboratory of Atmospheric Chemistry, CH-5232 Villigen,
Switzerland
[2] Onera -The French Aerospace Lab, F-91123 Palaiseau, France
[3] University of Helsinki, Department of Physics, P.O.Box 64, 00014 University of Helsinki,
Finland
[4] University of Innsbruck, Institute of Ion Physics and Applied Physics, Technikerstraße 25,
6020 Innsbruck, Austria
[5] University of Vienna, Faculty of Physics, Boltzmanngasse 5, 1090 Vienna, Austria
[6] Institute for Atmospheric and Environmental Sciences, Goethe University Frankfurt, 60438
Frankfurt am Main, Germany
[7] Universidade de Lisboa, Ed. C8, Campo Grande, Lisboa- 1749-016, Portugal
[8] CERN, CH-1211 Geneva, Switzerland
[9] Tofwerk AG, 3600 Thun, Switzerland
[10] School of Earth and Environmental Sciences, University of Manchester, Manchester M13
9PL, UK
[11] IDL -Universidade da Beira Interior, Av. Marquês D'Avila e Bolama, 6201-001 Covilhã,
Portugal.
[12] Center for Atmospheric Particle Studies, Carnegie Mellon University, Pittsburgh,
Pennsylvania 15213, USA

37   [13] Division of Chemistry and Chemical Engineering, California Institute of Technology,
38   Pasadena, California 91125, USA
39   [14] University of Eastern Finland, FI-70211 Kuopio, Finland
40   [15] Aerodyne Research Inc., Billerica, Massachusetts 01821, USA
41   [16] Department of Atmospheric and Oceanic Sciences, University of Colorado, Boulder,
42   Colorado 80309-0311, USA.
43

44

45

Abstract

46   **Abstract**

47   It was recently shown by the CERN CLOUD experiment that biogenic highly oxygenated

48   molecules (HOMs) form particles under atmospheric conditions in the absence of sulfuric

49   acid where ions enhance the nucleation rate by one to two orders of magnitude. The biogenic

50   HOMs were produced from ozonolysis of α-pinene at 5°C. Here we extend this study to

51   compare the molecular composition of positive and negative HOM clusters measured with

52   atmospheric pressure interface time-of-flight mass spectrometers (APi-TOFs), at three

53   different temperatures (25°C, 5°C and -25°C). Most negative HOM clusters include a nitrate

54   (NO_3^-) ion and the spectra are similar to those seen in the nighttime boreal forest. On the

55   other hand, most positive HOM clusters include an ammonium (NH_4^+) ion and the spectra are

56   characterized by mass bands that differ in their molecular weight by ~20 C atoms,

57   corresponding to HOM dimers. At lower temperatures the average oxygen to carbon (O:C)

58   ratio of the HOM clusters decreases for both polarities, reflecting an overall reduction of

59   HOM formation with decreasing temperature. This indicates a decrease in the rate of

60   autoxidation with temperature due to a rather high activation energy as has previously been

61   determined by quantum chemical calculations. Furthermore, at the lowest temperature

62   (-25°C) the presence of C_{30} clusters show that HOM monomers start to contribute to the

63   nucleation of positive clusters. These experimental findings are supported by quantum

64   chemical calculations of the binding energies of representative neutral and charged clusters.

1. Introduction

66   Atmospheric aerosol particles directly affect climate by influencing the transfer of radiant

67   energy through the atmosphere (Boucher et al., 2013). In addition, aerosol particles can

Atmospheric
Chemistry
and Physics
Discussions

Open Access

68   indirectly affect climate, by serving as cloud condensation nuclei (CCN) and ice nuclei (IN).

69   They are of natural or anthropogenic origin, and result from direct emissions (primary

70   particles) or from oxidation of gaseous precursors (secondary particles). Understanding

71   particle formation processes in the atmosphere is important since more than half of the

72   atmospheric aerosol particles may originate from nucleation (Dunne et al., 2016; Merikanto

73   et al., 2009).

74   Due to its widespread presence and low saturation vapor pressure, sulfuric acid is believed to

75   be the main vapor responsible for new particle formation (NPF) in the atmosphere. Indeed,

76   particle nucleation is dependent on its concentration, albeit with large variability (Kulmala et

77   al., 2004). The combination of sulfuric acid with ammonia and amines increases nucleation

78   rates due to a higher stability of the initial clusters (Almeida et al., 2013; Kirkby et al., 2011;

79   Kürten et al., 2016). However, these clusters alone cannot explain the particle formation rates

80   observed in the atmosphere. Nucleation rates are greatly enhanced when oxidized organics

81   are present together with sulfuric acid, resulting in NPF rates that closely match those

82   observed in the atmosphere (Metzger et al., 2010; Riccobono et al., 2014). An important

83   characteristic of the organic molecules participating in nucleation is their high oxygen content

84   and consequently low vapor pressure. The formation of these highly oxygenated molecules

85   (HOMs) has been described by Ehn et al. (2014), who found that, following the well-known

86   initial steps of α-pinene ozonolysis through a Criegee intermediate leading to the formation of

87   an $RO_2\cdot$ radical, several repeated cycles of intramolecular hydrogen abstractions and O_2

88   additions produce progressively more oxygenated $RO_2\cdot$ radicals, a mechanism called

89   autoxidation (Crounse et al., 2013). The (extremely) low volatility of the HOMs results in

90   efficient NPF and growth, even in the absence of sulfuric acid (Kirkby et al., 2016; Tröstl et

91   al., 2016). The chemical composition of HOMs during NPF has been identified from α-

92   pinene and pinanediol oxidation by Praplan et al. (2015) and Schobesberger et al. (2013),

93   respectively.

94   Charge has also been shown to enhance nucleation (Kirkby et al., 2011). Ions are produced

95   in the atmosphere mainly by galactic cosmic rays and radon. The primary ions are N^+, N_2^+,

96   O^+, O_2^+, H_3O^+, O^- and O_2^- (Shuman et al., 2015). These generally form clusters with water

97   (e.g. $(H_2O)H_3O^+$) and after further collisions the positive and negative charges are transferred

98   to trace species with highest and lowest proton affinities, respectively (Ehn et al., 2010). Ions

Atmospheric
Chemistry
and Physics
Discussions

99   are expected to promote NPF by increasing the cluster binding energy and reducing

100   evaporation rates (Hirsikko et al., 2011). Recent laboratory experiments showed that ions

101   increase the nucleation rates of HOMs from the oxidation of α-pinene by one to two orders of

102   magnitude compared to neutral conditions (Kirkby et al. 2016). This is due to two effects, of

103   which the first is more important: 1) an increase in cluster binding energy, which decreases

104   evaporation and 2) an enhanced collision probability, which increases the condensation of

105   polar vapors on the charged clusters (Lehtipalo et al., 2016; Nadykto, 2003).

106   Temperature plays an important role in nucleation, resulting in strong variations of NPF

107   at different altitudes. Kürten et al. (2016) studied the effect of temperature on nucleation for

108   the sulfuric acid - ammonia system, finding that low temperatures decrease the needed

109   concentration of H_2SO_4 to maintain a certain nucleation rate. Similar results have been found

110   for sulfuric acid – water binary nucleation (Duplissy et al., 2016; Merikanto et al., 2016),

111   where temperatures below 0˚C were needed for NPF to occur at atmospheric concentrations.

112   Up to now, no studies have addressed the temperature effect on NPF driven by HOMs from

113   biogenic precursors such as α-pinene.

114   In this study we focus on the chemical characterization of the ions and the influence of

115   temperature on their chemical composition during organic nucleation in the absence of

116   sulfuric acid. The importance of such sulfuric acid-free clusters for NPF has been shown in

117   the laboratory (Kirkby et al., 2016; Tröstl et al., 2016) as well as in the field (Bianchi et al.,

118   2016). We present measurements of the NPF process from the detection of primary ions (e.g.

119   N_2^+, O_2^+, NO^+) to the formation of clusters in the size range of small particles, all under

120   atmospherically relevant conditions. The experiments were conducted at three different

121   temperatures (-25, 5 and 25 ˚C) enabling the simulation of pure biogenic NPF representative

122   of different tropospheric altitudes.

123

2. Methods

2.1. The CLOUD chamber

126   We conducted experiments at the CERN CLOUD chamber (Cosmics Leaving Outdoor

127   Droplets). With a volume of 26.1 m^3, the chamber is built of electropolished stainless steel

128   and equipped with a precisely controlled gas system. The temperature inside the chamber is

129   measured with a string of six thermocouples (TC, type K) which were mounted horizontally

130   between the chamber wall and the center of the chamber at distances of 100, 170, 270, 400,

131   650, and 950 mm from the chamber wall (Hoyle et al., 2016). The temperature is controlled

132   accurately (with a precision of $\pm$ 0.1°C) at any tropospheric temperature between -65 and

133   30 °C (in addition, the temperature can be raised to 100 °C for cleaning). The chamber

134   enables atmospheric simulations under highly stable experimental conditions with low

135   particle wall loss and low contamination levels (more details of the CLOUD chamber can be

136   found in Kirkby et al. (2011) and Duplissy et al. (2016)). Before the start of the experiments

137   the CLOUD chamber was cleaned by rinsing the walls with ultra-pure water, followed by

138   heating to 100°C and flushing at a high rate with humidified synthetic air and elevated ozone

139   (several ppmv) (Kirkby et al., 2016). This resulted in SO_2 and H_2SO_4 concentrations that

140   were below the detection limit (<15 pptv and $<5 \times 10^4$ cm^{-3}, respectively), and total organics

141   (largely comprising high volatility C_1–C_3 compounds) that were below 150 pptv.
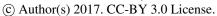
142   The air in the chamber is ionized by galactic cosmic rays (GCR); higher ion generation

143   rates can be induced by a pion beam (π^+) from the CERN Proton Synchrotron enabling

144   controlled simulation of galactic cosmic rays throughout the troposphere. Therefore, the total

145   ion-pair production rate in the chamber is between 2 (no beam) and 100 cm^{-3} s^{-1} (maximum

146   available beam intensity, Franchin et al., 2015).

147   2.2. **Instrumentation**

148   The main instruments employed for this study were atmospheric pressure interface time-

149   of-flight (APi-TOF, Aerodyne Research Inc. & Tofwerk AG) mass spectrometers. The APi-

150   TOF is able to measure the intensity of positive or negative ions and cluster ions over a wide

151   range of mass-to-charge ratios at concentrations relevant for the ambient atmosphere. The

152   instrument has two main parts. The first is the atmospheric pressure interface (APi) where

153   ions are transferred from atmospheric pressure to low pressures via three differentially

154   pumped vacuum stages. Ions are focused and guided by two quadrupoles and ion lenses. The

155   second is the time-of-flight mass analyzer (TOF), where the pressure is approximately 10^{-6}

156   mbar. The sample flow from the chamber was 10 L/min and the core-sampled flow into the

157   APi was 0.8 L/min, with the remaining flow being discarded.

158   We calibrated the APi-TOF using trioctylmethylammonium bis (trifluoromethylsulfonyl)

159   imide (TBMA, $C_{27}H_{54}F_6N_2O_4S_2$) to facilitate the exact ion mass determination in both

160   positive and negative ion modes. We employed two calibration methods, the first one by

161   nebulizing TBMA and separating cluster ions with a high-resolution ultra-fine differential

162   mobility analyzer (UDMA) (see Steiner et al. (2014) for more information); the second one

163   by using electrospray ionization of a TBMA solution. The calibration with the electrospray

164   ionization was performed three times, one for each temperature. These calibrations enabled

165   mass/charge (m/z) measurements with high accuracy up to 1500 Th in the positive ion mode

166   and 900 Th in the negative ion mode.

167   Additionally, two peaks in the positive ion mode were identified as contaminants and also

168   used for calibration purposes at the three different temperatures: $C_{10}H_{14}OH^+$ and $C_{20}H_{28}O_2H^+$.

169   These peaks were present before the addition of ozone in the chamber (therefore being most

170   likely not products of α-pinene ozonolysis) and were also detected by a proton transfer

171   reaction time of flight mass spectrometer (PTR-TOF-MS). Both peaks appeared at the same

172   m/z at all three temperatures. Therefore, based on the calibrations with the UDMA, the

173   electrospray and the two organic calibration peaks, we expect an accurate mass calibration at

174   the three temperatures.

175   2.3. **Experimental conditions**

176   All ambient ion composition data reported here were obtained during nucleation

177   experiments from pure α-pinene ozonolysis. The experiments were conducted under dark

178   conditions, at a relative humidity (RH) of 38% with an O_3 mixing ratio between 33 and 43

179   ppbv (Table 1). The APi-TOF measurements were made under both galactic cosmic ray

180   (GCR) and π^+ beam conditions, with ion-pair concentrations around 700 cm^{-3} and 4000 cm^{-3},

181   respectively.

182

183

184

Atmospheric
Chemistry
and Physics
Discussions

185   Table 1. Experiments performed at the CLOUD chamber.

Campaign	Experiment No.	Ionization	α-pinene (pptv)	O_3 (ppbv)	Mass spectrometer polarity	Temperature (˚C)
CLOUD 8	1211.02	GCR	258	33.8	Negative	5
CLOUD 10	1710.04	π^+ beam	618	41.5	Positive	5
CLOUD 10	1712.04	π^+ beam	511	40.3	Negative and positive	25
CLOUD 10	1727.04	π^+ beam	312	43.3	Negative and positive	-25

186

2.4. Quantum chemical calculations

188   Quantum chemical calculations were performed on the cluster ion formation from the
189   oxidation products of α-pinene. The Gibbs free energies of formation of representative HOM
190   clusters were calculated using the MO62X functional (Zhao and Truhlar, 2008), and the 6-
191   31+G(d) basis set (Ditchfield, 1971) using the Gaussian09 program (Frisch et al., 2009). This
192   method has been previously applied for clusters containing large organic molecules (Kirkby
193   et al., 2016).

194

3. Results and discussion

3.1. Ion composition

197   Under relatively dry conditions, the main detected positive ions were N_2H^+ and O_2^+. With
198   increasing RH we observed the water clusters H_3O^+, $(H_2O)\cdot H_3O^+$ and $(H_2O)_2\cdot H_3O^+$ as well as
199   NH_4^+, $C_5H_5NH^+$ (protonated pyridine), Na^+, and K^+. The concentrations of the precursors of
200   some of the latter ions are expected to be very low: for example, NH_3 mixing ratios were
201   previously found to be in the range of 0.3 pptv (at −25 ˚C), 2 pptv (at 5 ˚C) and 4.3 pptv (at
202   25 ˚C) (Kürten et al., 2016). For the negative ions, NO_3^- was the main detected background
203   signal. Before adding any trace gas to the chamber the signal of HSO_4^- was at a level of 1%
204   of the NO_3^- signal (corresponding to $<5\cdot10^{-4}$ molecules cm^{-3}, Kirkby et al., 2016), excluding
205   any contribution of sulfuric acid to nucleation in our experiments.

Atmospheric
Chemistry
and Physics
Discussions

Open Access

EGU

206   After initiating α-pinene ozonolysis, more than 460 organic ions were identified in the

207   positive spectrum. The majority of peaks were clustered with NH_4^+, while only 10.2 % of the

208   identified peaks were composed of protonated organic molecules. In both cases the organic

209   core was of the type $C_{7-10}H_{10-16}O_{1-10}$ for the monomer region and $C_{17-20}H_{24-32}O_{5-19}$ for the

210   dimer region.

211   In the negative spectrum we identified more than 530 HOMs, of which ~62%

212   corresponded to organic clusters with NO_3^- or, to a lesser degree, $HNO_3 \cdot NO_3^-$. The rest of

213   the peaks were negatively charged organic molecules. In general, the organic core of the

214   molecules was of the type $C_{7-10}H_{9-16}O_{3-12}$ in the monomer region and $C_{17-20}H_{19-32}O_{10-20}$ in the

215   dimer region. For brevity we refer to the monomer, dimer (and n-mer) as C_{10}, C_{20} and $C_{(10n)}$

216   respectively. Here, the subscript indicates the maximum number of carbon atoms in these

217   molecules, even though the bands include species with slightly fewer carbon atoms.

218

3.1.1.   Positive spectrum

220   The positive spectrum is characterized by bands of high intensity at C_{20} intervals, as

221   shown in Figure 1B. Although we detected the monomer band (C_{10}), its integrated intensity

222   was much lower than the C_{20} band; furthermore, the trimer and pentamer bands were almost

223   completely absent. Based on chemical ionization mass spectrometry measurements, Kirkby et

224   al. (2016) calculated that the HOM molar yield at 5°C was 3.2% for the ozonolysis of α-

225   pinene, with a fractional yield of 10 to 20% for dimers. A combination reaction of two

226   oxidized peroxy radicals has been previously reported to explain the rapid formation of

227   dimers resulting in covalently bound molecules (see Section 3.3). The pronounced dimer

228   signal with NH_4^+ indicates that (low-volatility) dimers are necessary for positive ion

229   nucleation and initial growth. We observe growth by dimer steps up to C_{80} and possibly even

230   C_{100}. A cluster of two dimers, C_{40}, with a mass/charge in the range of ~ 700 - 1100 Th, has a

231   mobility diameter around 1.5 nm (based on Ehn et al. (2011)).

232   Our observation of HOMs-NH_4^+ clusters implies strong hydrogen bonding between

233   the two species. This is confirmed by quantum chemical calculations which shall be

234   discussed in Section 3.3. Although hydrogen bonding could also be expected between HOMs

235   and H_3O^+, we do not observe such clusters. This probably arises from the higher proton

Atmospheric
Chemistry
and Physics
Discussions

236   affinity of NH_3, 203.6 kcal/mol, compared with H_2O, 164.8 kcal/mol (Hunter and Lias,

237   1998). Thus, most H_3O^+ ions in CLOUD will transfer their proton to NH_3 to form NH_4^+.
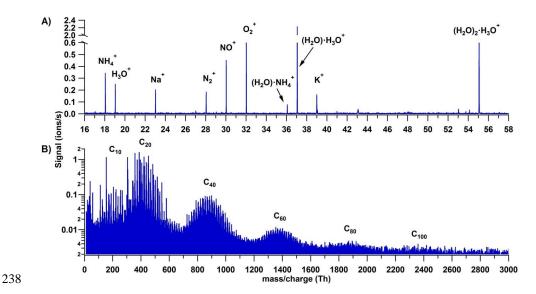

239   Figure 1. Positive spectra at 5˚C. A) Low mass region, where primary ions from galactic
240   cosmic ray are observed, as well as secondary ions such as NH_4^+ which are formed by charge
241   transfer to contaminants. B) Higher mass region during pure biogenic nucleation, which
242   shows broad bands in steps of C_{20}. Most of the peaks represent clusters with NH_4^+.

243

3.1.2.   Negative spectrum

245   In the negative spectra, the monomer, dimer and trimer bands are observed during

246   nucleation (Fig. 2). Monomers and dimers have similar signal intensities, whereas the trimer

247   intensity is at least 10 times lower (Figure 2A and B). The trimer signal is reduced since it is

248   a cluster of two gas phase species (C_{10}+C_{20}). Additionally, a lower transmission in the APi-

249   TOF may also be a reason for the reduced signal.

250   In Fig. 2, we compare the CLOUD negative-ion spectrum with the one from nocturnal

251   atmospheric measurements from the boreal forest at Hyytiälä as reported by Ehn et al. (2010).

252   Panels 2A and 2B show the negative spectrum of α-pinene ozonolysis in the CLOUD

253   chamber on logarithmic and linear scales, respectively. Panel 2C shows the Hyytiälä

254   spectrum for comparison. Although the figure shows unit mass resolution, the high resolution

255   analysis confirms the identical composition for the main peaks: $C_8H_{12}O_7 \cdot NO_3^-$,

256    $C_{10}H_{14}O_7 \cdot NO_3^-$, $C_{10}H_{14}O_8 \cdot NO_3^-$, $C_{10}H_{14}O_9 \cdot NO_3^-$, $C_{10}H_{16}O_{10} \cdot NO_3^-$ and $C_{10}H_{14}O_{11} \cdot NO_3^-$

257   (marked in the monomer region), and $C_{19}H_{28}O_{11} \cdot NO_3$, $C_{20}H_{32}O_{13} \cdot NO_3^-$, $C_{19}H_{28}O_{13} \cdot NO_3^-$,

258    $C_{20}H_{32}O_{13} \cdot NO_3^-$, $C_{20}H_{30}O_{14} \cdot NO_3^-$, $C_{20}H_{30}O_{14} \cdot NO_3^-$, $C_{20}H_{30}O_{16} \cdot NO_3^-$ and $C_{20}H_{30}O_{18} \cdot NO_3^-$

259   (marked in the dimer region). The close correspondence in terms of composition of the main

260   HOMs from the lab and the field both in the monomer and dimer region indicates a close

261   reproduction of the atmospheric night-time conditions at Hyytiälä by the CLOUD

262   experiment. In both cases the ion composition was dominated by HOMs clustered with NO_3^-.

263   However, Ehn et al. (2010) did not report nocturnal nucleation, possibly because of a higher

264   ambient condensation sink than in the CLOUD chamber.

265

266   Figure 2. Comparison of the negative ion composition during α-pinene ozonolysis in CLOUD
267   and during night time in the boreal forest at Hyytiälä (Finland). A) CLOUD spectrum on a
268   logarithmic scale. B) CLOUD spectrum on a linear scale. C) Typical night time spectrum
269   from the boreal forest at Hyytiälä (Finland), adapted from Ehn et al. (2010).

270

Atmospheric
Chemistry
and Physics
Discussions

Open Access

3.2. **Temperature dependence**

271

272 Experiments at three different temperatures (25 °C, 5°C and -25 ˚C) were conducted
273 at similar relative humidity and ozone mixing ratios (Table 1 and Figure 3). Mass defect plots
274 are shown for the same data in Figure 4. The mass defect is the difference between the exact
275 and the integer mass and is shown on the y-axis versus the mass/charge on the x-axis. Each
276 point represents a distinct atomic composition of a molecule or cluster. Although the
277 observations described in the following are valid for both polarities, the positive ion mode
278 shows the differences in the chemistry at the three temperatures more clearly.

279 The first point to note is the change in the distribution of the signal intensity seen in
280 Figure 3 (height of the peaks) and in Figure 4 (size of the dots) with temperature. In the
281 positive ion mode, the dimer band has the highest intensity at 25 and 5˚C, while at -25˚C the
282 intensity of the monomer becomes comparable to that of the dimer. This indicates a reduced
283 rate of dimer formation at -25 ˚C, or that the intensity of the ion signal depends on both the
284 concentration of the neutral compound and on the stability of the ion cluster. Although the
285 monomer concentration is higher than that of the dimers (Tröstl et al., 2016), the C_{20} ions are
286 the more stable ion clusters as they can form more easily two hydrogen bonds with NH_4^+ (see
287 Section 3.3). Thus, positive clusters formed from monomers may not be stable enough at
288 higher temperatures. Moreover, charge transfer to dimers is also favored.
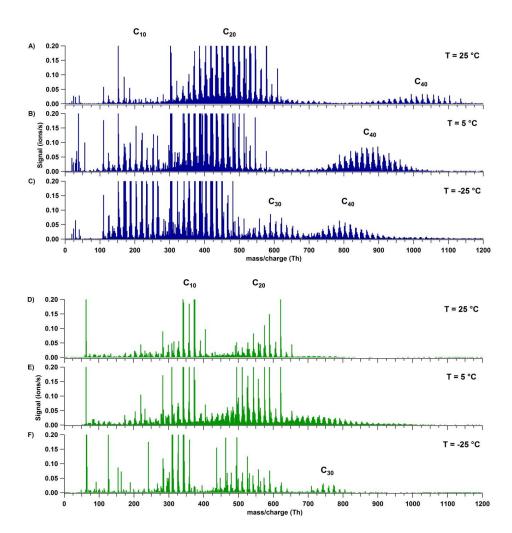
Figure 3. Positive (A-C) and negative (D-F) mass spectra during pure biogenic nucleation induced by ozonolysis of ▯-pinene) at three temperatures: 25˚C (A, D), 5˚C (B, E) and -25˚C (C, F). A progressive shift towards a lower oxygen content and lower masses is observed in all bands as the temperature decreases. Moreover, the appearance of C_{30} species can be seen in the positive spectrum at the lowest temperature (C).

The data also show a "shift" in all band distributions towards higher masses with increasing temperature, denoting a higher concentration of the more highly oxygenated molecules and the appearance of progressively more oxygenated compounds at higher temperatures. The shift is even more pronounced in the higher mass bands, as clearly seen in

300   the C_{40} band of the positive ion mode in Figure 3 (A-C). In this case the combination of two

301   HOM dimers to a C_{40} cluster essentially doubles the shift of the band towards higher

302   mass/charge at higher temperatures compared to the C_{20} band. Moreover, the width of each

303   band increases with temperature, as clearly seen in the positive ion mode in Figure 4,

304   especially for the C_{40} band. At high temperatures, the production of more highly oxygenated

305   HOMs seems to increase the possible combinations of clusters, resulting in a wider band

306   distribution.

307

308

309   Figure 4. Mass defect plots with the color code denoting the O:C ratio (of the organic core) at
310   25, 5 and -25°C for positive (A-C) and negative ion mode (D-F). A lower O:C ratio is
311   observed in the positive ion mode than in the negative ion mode. The intensity of the main
312   peaks (linearly proportional to the size of the dots) changes with temperature for both
313   polarities due to a lower degree of oxygenation at lower temperature.

314

315   This trend in the spectra indicates that the unimolecular autoxidation reaction

316   accelerates at higher temperatures in competition to the bimolecular termination reactions

317   with HO_2 and RO_2. This is expected. If unimolecular and bimolecular reactions are

318   competitive, the unimolecular process will have a much higher barrier because the pre-

319   exponential term for a unimolecular process is a vibrational frequency while the pre-

320   exponential term for the bimolecular process is at most the bimolecular collision frequency,

321   which is four orders of magnitude lower. Quantum chemical calculations determine

Atmospheric
Chemistry
and Physics
Discussions

Open Access

322   activation energies between 22.56 and 29.46 kcal/mol for the autoxidation of different RO_2

323   radicals from α-pinene (Rissanen et al., 2015). Thus, such a high barrier will strongly reduce

324   the autoxidation rate at the low temperatures.

325   The change in the rate of autoxidation is also reflected in the O:C ratio, both in the

326   positive ion mode (Figure 4 A-C), and the negative ion mode (D-F), showing a clear increase

327   with increasing temperature. The average O:C ratios (weighted by the peak intensities) are

328   presented in Table 2 for both polarities and the three temperatures, for all the identified peaks

329   (total) and separately for the monomer and dimer bands For a temperature change from 25 to

330   -25°C the O:C ratio decreases for monomers, dimers and total number of peaks. At high

331   masses (e.g., for the C_{30} and C_{40} bands), the O:C ratio may be slightly biased since accurate

332   identification of the molecules is less straightforward: as an example, $C_{39}H_{56}O_{25} \cdot NH_4^+$ has an

333   exact mass of 942.34 Th (O/C = 0.64), which is very similar to $C_{40}H_{60}O_{24} \cdot NH_4^+$ at 942.38 Th

334   (O/C = 0.60). However, such possible misidentification would not influence the calculated

335   total O/C by more than 0.05, and the main conclusions presented here remain robust.

336

337   Table 2. Signal weighted average O:C ratios for positive and negative
338   spectra at 25, 5 and -25 °C.

Temperature (°C)	*O/C*					
	Positive mode			*Negative mode*		
	Monomer	*Dimer*	*Total*	*Monomer*	*Dimer*	*Total*
25	0.37	0.57	0.54	0.94	0.81	0.90
5	0.34	0.51	0.49	0.88	0.66	0.75
-25	0.31	0.38	0.36	0.79	0.65	0.68

339

340   The O:C ratios are higher for the negative ions than for the positive ions at any of the

341   three temperatures. Although some of the organic cores are the same in the positive and

342   negative ion mode, the intensity of the peaks of the most oxygenated species is higher in the

343   negative spectra. While the measured O:C ratio ranges between 0.4 and 1.2 in the negative

344   ion mode, it is between 0.1 and 1.2 in the positive ion mode. An O:C ratio of 0.1, which was

345   detected only in the positive ion mode, corresponds to monomers with 1 oxygen atom or

346   dimers with two oxygen atoms. The presence of molecules with such low oxygen content was

Atmospheric
Chemistry
and Physics
Discussions

347   also confirmed with a proton transfer reaction time-of-flight mass spectrometer (PTR-TOF-

348   MS), at least in the monomer region. The ions with this low O:C ratio are probably from the

349   known main oxidation products like pinonaldehyde, pinonic acid, etc. It is likely that these

350   molecules, which were detected only in the positive mode, contribute only to the growth of

351   the newly formed particles (if at all) rather than to nucleation, owing to their high volatility

352   (Tröstl et al., 2016). In this sense, the positive spectrum could reveal both the molecules that

353   participate in the new particle formation and those that contribute to growth. The differences

354   in the O:C ratios between the two polarities are a result of the affinities of the organic

355   molecules to form clusters either with NO_3^- or NH_4^+, which, in turn, depends on the

356   molecular structure and the functional groups. Hyttinen et al. (2015) reported the binding

357   energies of selected highly oxygenated products of cyclohexene detected by a nitrate CIMS,

358   finding that the addition of OOH groups to the HOM strengthens the binding of the organic

359   core with NO_3^-. Even when the number of H-bonds between NO_3^- and HOM remains the

360   same, the addition of more oxygen atoms to the organic compound could strengthen the

361   bonding with the NO_3^- ion. Thus, the less oxygenated HOMs were not detected in those

362   experiments, neither in ours, in the negative mode. The binding energies were calculated for

363   the positive mode HOMs-NH_4^+ and are discussed in Section 3.3.

364   We also tested to which extent the formation of the C_{40} band could be reproduced by

365   permutation of the potential C_{20} clusters weighted by the dimer signal intensity. Figure 5

366   shows the measured spectrum (blue) and two types of modeled tetramers: one combining all

367   peaks from the C_{20} band (light gray) and one combining only those peaks with an organic

368   core with O/C ≥ 0.4, i.e. likely non-volatile molecules (dark gray). The better consistency of

369   the latter with the measured tetramer band suggests that only the molecules with O/C ≥ 0.4

370   are able to form the tetramer cluster. This would mean that C_{20} molecules with 2-7 oxygen

371   atoms are likely not to contribute to the nucleation, but only to the growth of the newly

372   formed particles.

373

Atmospheric
Chemistry
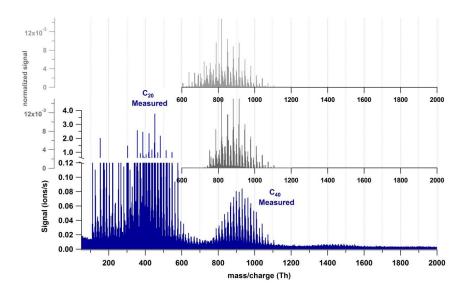and Physics
Discussions

374

Figure 5. Comparison of the positive ion mode spectrum measured (blue), the C_{40} band obtained by the combination of all C_{20} molecules (light gray) and the C_{40} band obtained by combination of only the C_{20} molecules with O/C ≥ 0.4 (dark gray). The low or absent signals at the lower masses obtained by permutation suggests that only the highly oxygenated dimers are able to cluster and form C_{40}.

380

These two observations (change in signal distribution and band "shift") are not only valid for positive and negative ions, but also for the neutral molecules as observed by two nitrate chemical-ionization atmospheric-pressure-interface time-of-flight mass spectrometers (CI-APi-TOF; Aerodyne Research Inc. and Tofwerk AG). This confirms that there is indeed a change in the HOM composition with different temperature rather than a charge redistribution effect which would only be observed for the ions (APi-TOF). The detailed analysis of the neutral molecules detected by these CI-APi-TOFs will be subject of another paper and is not discussed here.

A third distinctive trend in the positive mode spectra at the three temperatures is the increase in signal intensity of the C_{30} band at -25˚C. The increase in the signal of the trimer also seems to occur in the negative ion mode when comparing panels D and F in Figure **3**. For this polarity, data from two campaigns were combined (Table **1**). To avoid a bias by possible differences in the APi-TOF settings, we only compare the temperatures from the same campaign, CLOUD 10, therefore experiments at 25 ˚C and -25 ˚C. The increase in the

Atmospheric
Chemistry
and Physics
Discussions

395   trimer signal may be due to greater stability of the monomer-dimer clusters or even of three

396   C_{10} molecules at low temperatures, as further discussed below.

397

398   3.3. **Quantum chemical calculations**

399   Three points were addressed in the quantum chemical calculations to elucidate the most

400   likely formation pathway for the first clusters, and its temperature dependence. These

401   included (i) the stability of the organic cores with NO_3^- and NH_4^+ depending on the binding

402   functional group, (ii) the difference between charged and neutral clusters in terms of

403   clustering energies, and finally (iii) the possible nature of clusters in the dimer and trimer

404   region.

405   The calculations showed that among the different functional groups the best interacting

406   groups with NO_3^- are in order of importance carboxylic acids (R–C(=O)–OH), hydroxyls (R–

407   OH), peroxy acids (R–C(=O)–O–OH), hydroperoxides (R–O–OH) and carbonyls (R–(R'–)

408   C=O). On the other hand, NH_4^+ preferably forms a hydrogen bond with the carbonyl group

409   independent of which functional group the carbonyl group is linked to: Figure 6 shows

410   examples of NH_4^+ clusters with corresponding free energies of formation for carbonyls ($\Delta G=$

411   -17.98 kcal/mol), carboxylic acid ($\Delta G=$ -17.32 kcal/mol), and peroxy acid ($\Delta G=$ -17.46

412   kcal/mol). For the three examples shown, the interaction of one hydrogen from NH_4^+ with a

413   C=O group is already very stable with a free energy of cluster ion formation close to -18

414   kcal/mol.

415

416

Atmospheric
Chemistry
and Physics
Discussions

A

ΔG = -17,98 kcal/mol

B

ΔG = -17,32 kcal/mol

C

ΔG = -17,46 kcal/mol

417
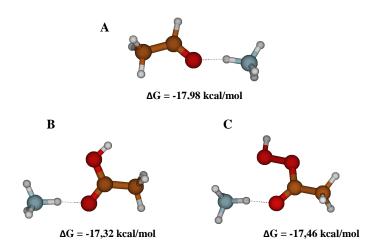
Figure 6. Quantum chemical calculations of the free energy related to the cluster formation
418   between NH_4^+ and three structurally similar molecules with different functional groups: A)
acetaldehyde, B) acetic acid and C) peracetic acid.

419

420   To evaluate the effect of the presence of a second C=O to the binding of the organic

421   compound with NH_4^+, we performed a series of calculations with a set of surrogates

422   containing two C=O groups separated by a different number of atoms, as shown in Figure 7.

423   The addition of a second functional group allows the formation of an additional hydrogen-

424   bond, increasing the stability of the cluster considerably (almost two folds) from about -18

425   kcal/mol to -34.07 kcal/mol, whereby the position of the second functional group to form an

426   optimal hydrogen bond (with a 180° angle for N-H-O) strongly influences the stability of the

427   cluster, as can be seen in Figure 7. Thus, optimal separation and conformational flexibility of

428   functional groups is needed to enable an effective formation of two hydrogen bonds with

429   NH_4^+. This could be an explanation for the observation that the signal intensity is higher for

430   dimers than for monomers, as dimers can more easily form two optimal hydrogen bonds with

431   NH_4^+.

432

433

434

Atmospheric
Chemistry
and Physics
Discussions

435

ΔG = -17,32 kcal/mol

ΔG = -20,81 kcal/mol   ΔG = -23,43 kcal/mol
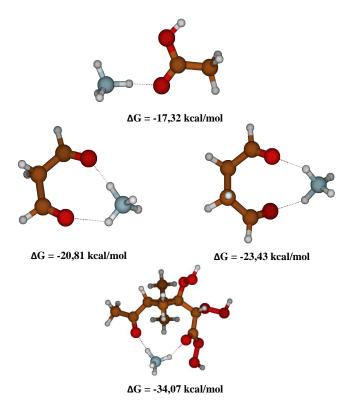
ΔG = -34,07 kcal/mol

436

Figure 7. Quantum chemical calculations for different organic molecules with a
carbonyl as the interacting functional group with NH_4^+. Increasing the interacting
437   groups from one to two increases the stability of the cluster. The distance between the
interacting groups also influences the cluster stability.

438

439   As shown by Kirkby et al. (2016), ions increase the nucleation rates by one to two

440   orders of magnitudes compared to neutral nucleation. This is expected due to the strong

441   electrostatic interaction between charged clusters. To understand how the stability difference

442   relates to the increase in the nucleation rate, the ΔGs of charged and neutral clusters were

443   compared. For this, $C_{10}H_{14}O_7$ and $C_{20}H_{30}O_{14}$ were selected as representative molecules of the

444   monomer and dimer region, respectively (Kirkby et al., 2016). Table 3 shows the calculated

445   free energies of formation (ΔG) of neutral, positive and negative clusters from these C_{10} and

446   C_{20} molecules at the three temperatures of the experiment. Results show that at 5°C, for

Atmospheric
Chemistry
and Physics
Discussions

447   example, ΔG of the neutral dimer ($C_{10} + C_{10}$) is -5.76 kcal/mol while it decreases to -20.95

448   kcal/mol when a neutral and a negative ion form a cluster ($C_{10} + C_{10}^-$). Similarly, trimers

449   show a substantial increase in stability when they are charged, i.e., from -2.15 kcal/mol to

450   -19.9 kcal/mol, for the neutral and negative cases, respectively. The reduced values of ΔG for

451   the charged clusters (positive and negative) indicate a substantial decrease in the evaporation

452   rate compared to that for neutral clusters, and, therefore, higher stability. Comparing the

453   NH_4^+ and NO_3^- clusters, the energies of formation for the monomer are -22.5 kcal/mol and

454   -25.99 kcal/mol, respectively, showing slightly higher stability for the negative cluster.

455   Inversely, the covalently bound dimer showed greater stability for the positive ion (-30.9

456   kcal/mol) compared to the negative ion (-25.65 kcal/mol).

457

458   Table 3. Gibbs free energies of cluster formation ΔG at three different temperatures. ΔG for
459   the molecules $C_{10}H_{14}O_7$ (C_{10}) and $C_{20}H_{30}O_{14}$ (C_{20}) forming neutral, as well as negative and
460   positive ion clusters.

	Cluster process	$\Delta G_{-25°C}$ (kcal/mol)	$\Delta G_{5°C}$ (kcal/mol)	$\Delta G_{25°C}$ (kcal/mol)
Neutral	$C_{10} + C_{10}$	-7.33	-5.76	-4.70
	$C_{10} + C_{20}$	-3.28	-2.15	-1.39
Positive	$C_{10} + NH_4^+$	-23.40	-22.50	-21.80
	$C_{20} + NH_4^+$	-31.80	-30.90	-30.20
	$C_{10} + C_{10} \cdot NH_4^+$	-12.90	-11.70	-10.90
	$C_{20} + C_{10} \cdot NH_4^+$	-26.00	-24.30	-23.30
	$C_{10} + C_{20} \cdot NH_4^+$	-17.60	-15.90	-14.80
Negative	$C_{10} + C_{10}^-$	-22.22	-20.95	-20.09
	$C_{20} + C_{10}^-$	-21.36	-19.90	-18.91
	$C_{10} + NO_3^-$	-27.27	-25.99	-25.14
	$C_{20} + NO_3^-$	-26.97	-25.65	-24.75
	$C_{10} + C_{10} \cdot NO_3^-$	-11.34	-10.09	-9.25

461

462   The temperature dependence of cluster formation is shown in Figure **8** for the positive ion

463   clusters. The blue and brown solid lines represent the needed ΔG for evaporation-collision

464   equilibrium at 0.3 pptv and 1 pptv HOM mixing ratio, respectively, calculated as described

465   by Ortega et al. (2012). The markers show the calculated formation enthalpies ΔG for each

466   of the possible clusters. For all cases, the trend shows an evident decrease in ΔG with

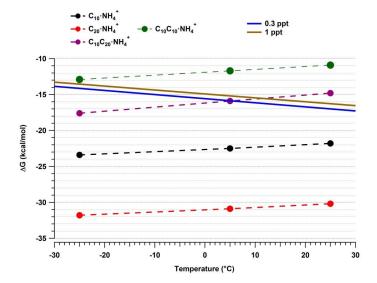467   decreasing temperature, with a correspondingly reduced evaporation rate.

468

Figure 8. Quantum chemical calculations of Gibbs free energies for cluster formation at -25, 5 and 25°C. Solid lines represent the required ΔG for equilibrium between evaporation and collision rates at 0.3 pptv and 1 pptv of the HOM mixing ratio, respectively. Markers show the ΔG for each cluster (organic core clustered with NH_4^+) at the three temperatures. $C_{10} \cdot NH_4^+$ (black circles) represent the monomer, $C_{20} \cdot NH_4^+$ (red circles) represent the covalently bound dimer, $C_{10}C_{10} \cdot NH_4^+$ (green circles) represent the dimer formed by the clustering of two monomers and $C_{10}C_{20} \cdot NH_4^+$ (purple circles) denote the preferential pathway for the trimer cluster (see Table 3).

At all three temperatures, the monomer cluster $C_{10} \cdot NH_4^+$ falls well below the equilibrium lines, indicating high stability. Even though the difference between -25°C and 25°C is just -1.6 kcal/mol in free energy, it is enough to produce a substantial difference in the intensity of the band, increasing the signal at least 8-fold at -25°C (as discussed in Section 3.2). In the case of the dimers, we consider the possibility of their formation by collision of a monomer $C_{10} \cdot NH_4^+$ with another C_{10} (resulting in a $C_{10}C_{10} \cdot NH_4^+$ cluster) or the dimer as $C_{20} \cdot NH_4^+$ cluster. The calculations show clearly that the cluster $C_{10}C_{10} \cdot NH_4^+$ is not stable at any of the three temperatures (green line). In contrast, the covalently-bound C_{20} forms very stable positive and negative ion clusters (see Table 3). Trimers are mainly observed at lower temperatures. Since the $C_{10}C_{10} \cdot NH_4^+$ cluster is not very stable, we discard the possibility of a trimer formation of the type $C_{10}C_{10}C_{10} \cdot NH_4^+$. Thus, the trimer is likely the combination of a monomer and a covalently-bound dimer ($C_{20}C_{10} \cdot NH_4^+$). According to our calculations (Table

21

Atmospheric
Chemistry
and Physics
Discussions

490   3) the preferred evaporation path for this cluster is the loss of C_{10} rather than the evaporation

491   of C_{20}. Therefore, we have chosen to represent only this path in Figure **8**. The ΔG of this

492   cluster crosses the evaporation-condensation equilibrium around 5 ˚C and 14 ˚C for a HOM

493   mixing ratio of 0.3 pptv and 1 pptv, respectively, in good agreement with the observed signal

494   increase of the trimer at -25°C (Figure 3 A-C). It is important to note that, due to the

495   uncertainty in the calculations, estimated to be $\leq$ 2 kcal/mol, we do not consider the crossing

496   as an exact reference.

497   The ΔG of the negative ion clusters, which are also presented in Table 3, decrease

498   similarly to the positive ion clusters by around 2 kcal/mol between 25˚C and -25˚C. The

499   cluster formation energies of the monomer and the dimer with NO_3^- are in agreement with the

500   observed comparable signal intensity in the spectrum (Figure 2) in a similar way as the

501   positive ion clusters. The covalently-bonded dimer ion $C_{20} \cdot NO_3^-$ is also more stable

502   compared to the dimer cluster $C_{10}C_{10} \cdot NO_3^-$, suggesting that the observed composition results

503   from covalently bonded dimers clustering with NO_3^- rather than two individual C_{10} clustering

504   to form a dimer.

505   The formation of a covalently bonded trimer seems unlikely, so the formation of highly

506   oxygenated molecules is restricted to the monomer and dimer region. The trimer could result

507   from the clustering of C_{10} and C_{20} species. Similarly, and based on the C_{20} pattern observed in

508   Figure 1B, we believe that the formation of the tetramer corresponds to the collision of two

509   dimers. No calculations were done for this case due to the complexity related to the sizes of

510   the molecules, which prevents feasible high level quantum chemical calculations.

511   Finally, the comparison between the ΔG values for charged and neutral clusters as

512   presented in Table 3 confirms the expected higher stability of ion clusters, decreasing the

513   evaporation rate of the nucleating clusters and enhancing new particle formation.

514

4. Conclusions

516   Ions observed during pure biogenic ion-induced nucleation were comprised of mainly

517   organics clustered with NO_3^- and NH_4^+ and to a lesser extent charged organic molecules only

518   or organics clustered with $HNO_3NO_3^-$. We found good correspondence between the negative

Atmospheric
Chemistry
and Physics
Discussions

519   ions measured in CLOUD with those observed in the boreal forest of Hyytiälä. The observed

520   similarity in the composition of the HOMs in the monomer and dimer region during new-

521   particle formation experiments at CLOUD suggests that pure biogenic nucleation might be

522   possible during night time if the condensation sink is sufficiently low, i.e., comparable to that

523   in the CLOUD chamber, where the wall loss rate for H_2SO_4 is $1.8 \cdot 10^{-3}$ s^{-1} (Kirkby et al.,

524   2016). The positive mass spectrum showed a distinctive pattern corresponding to progressive

525   addition of dimers (C_{20}), up to cluster sizes in the range of stable small particles.

526   Temperature strongly influenced the composition of the detected molecules in several

527   ways. With increasing temperature, a higher oxygen content (O:C ratio) in the molecules was

528   observed in both the positive and the negative mode. This indicates an increase in the

529   autoxidation rate of peroxy radicals which is in competition with their bimolecular

530   termination reactions with HO_2 and RO_2.

531   A broader range of organic molecules was found to form clusters with NH_4^+ than with

532   NO_3^-. Quantum chemical calculations using simplified molecules show that NH_4^+ preferably

533   forms a hydrogen bond with a carbonyl group independently of other functional groups

534   nearby. The addition of a second hydrogen bond was found to increase the cluster stability

535   substantially. Thus, the C_{20}-ions are the more stable ion clusters as they can form more easily

536   two hydrogen bonds with NH_4^+. Although molecules with low oxygen content were

537   measured in the C_{20} band (1 - 4 oxygen atoms), only the molecules with O/C $\geq$ 0.4 seem to be

538   able to combine to form larger clusters.

539   The quantum chemical calculations showed that the covalently-bonded dimer $C_{20} \cdot$

540   NO_3^- is also more stable than the dimer cluster $C_{10}C_{10} \cdot NO_3^-$, suggesting that the observed

541   composition results from covalently bonded molecules clustering with NO_3^- rather than C_{10}

542   clusters.

543   Temperature affected cluster formation by decreasing evaporation rates at lower

544   temperatures, despite of the lower O:C ratio. In the positive mode a pronounced growth of

545   clusters by addition of C_{20}-HOMs was observed. The formation of a C_{30}-cluster only

546   appeared at the lowest temperature, which was supported by quantum chemical calculations.

547   In the negative mode it appeared as well that the signal of the C_{30}-clusters became stronger

548   with lower temperature. The C_{40}- and higher clusters were probably not seen because of too

Atmospheric
Chemistry
and Physics
Discussions

Open Access

EGU

549 low sensitivity in this mass range due to the applied instrumental settings. More

550 measurements are needed to determine if the cluster growth of positive and negative ions

551 proceeds in a similar or different way.

552 **5. Acknowledgement**

577

Atmospheric
Chemistry
and Physics
Discussions

6. References

578   **6. References**

579   Almeida, J., Schobesberger, S., Kürten, A., Ortega, I. K., Kupiainen-Määttä, O., Praplan, A.
580   P., Adamov, A., Amorim, A., Bianchi, F., Breitenlechner, M., David, A., Dommen, J.,
581   Donahue, N. M., Downard, A., Dunne, E., Duplissy, J., Ehrhart, S., Flagan, R. C., Franchin,
582   A., Guida, R., Hakala, J., Hansel, A., Heinritzi, M., Henschel, H., Jokinen, T., Junninen, H.,
583   Kajos, M., Kangasluoma, J., Keskinen, H., Kupc, A., Kurtén, T., Kvashin, A. N., Laaksonen,
584   A., Lehtipalo, K., Leiminger, M., Leppä, J., Loukonen, V., Makhmutov, V., Mathot, S.,
585   McGrath, M. J., Nieminen, T., Olenius, T., Onnela, A., Petäjä, T., Riccobono, F., Riipinen, I.,
586   Rissanen, M., Rondo, L., Ruuskanen, T., Santos, F. D., Sarnela, N., Schallhart, S.,
587   Schnitzhofer, R., Seinfeld, J. H., Simon, M., Sipilä, M., Stozhkov, Y., Stratmann, F., Tomé,
588   A., Tröstl, J., Tsagkogeorgas, G., Vaattovaara, P., Viisanen, Y., Virtanen, A., Vrtala, A.,
589   Wagner, P. E., Weingartner, E., Wex, H., Williamson, C., Wimmer, D., Ye, P., Yli-Juuti, T.,
590   Carslaw, K. S., Kulmala, M., Curtius, J., Baltensperger, U., Worsnop, D. R., Vehkamäki, H.
591   and Kirkby, J.: Molecular understanding of sulphuric acid-amine particle nucleation in the
592   atmosphere., Nature, 502(7471), 359–63, doi:10.1038/nature12663, 2013.

593   Bianchi, F., Tröstl, J., Junninen, H., Frege, C., Henne, S., Hoyle, C. R., Molteni, U.,
594   Herrmann, E., Adamov, A., Bukowiecki, N., Chen, X., Duplissy, J., Gysel, M., Hutterli, M.,
595   Kangasluoma, J., Kontkanen, J., Kürten, A., Manninen, H. E., Münch, S., Peräkylä, O.,
596   Petäjä, T., Rondo, L., Williamson, C., Weingartner, E., Curtius, J., Worsnop, D. R., Kulmala,
597   M., Dommen, J. and Baltensperger, U.: New particle formation in the free troposphere: A
598   question of chemistry and timing, Science, 352 (6289), 1109–1112,
599   doi:10.1126/science.aad5456, 2016.

600   Boucher, O., Randall, D., Artaxo, P., Bretherton, C., Feingold, G., Forster, P., Kerminen, V.-
601   M. V.-M., Kondo, Y., Liao, H., Lohmann, U., Rasch, P., Satheesh, S. K., Sherwood, S.,
602   Stevens, B., Zhang, X. Y. and Zhan, X. Y.: Clouds and Aerosols. In: Climate Change 2013:
603   The Physical Science Basis. Contribution of Working Group I to the Fifth Assessment Report
604   of the Intergovernmental Panel on Climate Change., 571–657,
605   doi:10.1017/CBO9781107415324.016, 2013.

606   Crounse, J. D., Nielsen, L. B., Jørgensen, S., Kjaergaard, H. G. and Wennberg, P. O.:
607   Autoxidation of organic compounds in the atmosphere, J. Phys. Chem. Lett., 4(20), 3513–
608   3520, doi:10.1021/jz4019207, 2013.

609   Ditchfield, R.: Self-consistent molecular-orbital methods. IX. An extended gaussian-type
610   basis for molecular-orbital studies of organic molecules, J. Chem. Phys., 54 (2), 724,
611   doi:10.1063/1.1674902, 1971.

612   Dunne, E. M., Gordon, H., Andreas, K., Duplissy, J., Williamson, C., Ortega, I. K., Pringle,
613   K. J., Adamov, A., Baltensperger, U., Barmet, P., Benduhn, F., Bianchi, F., Breitenlechner,
614   M., Clarke, A., Curtius, J., Dommen, J., Donahue, N. M., Ehrhart, S., Flagan, R. C., Franchin,
615   A., Guida, R., Hakala, J., Hansel, A., Heinritzi, M., Jokinen, T., Kangasluoma, J., Kirkby, J.,
616   Kulmala, M., Kupc, A., Lawler, M. J., Lehtipalo, K., Makhmutov, V., Mathot, S., Miettinen,
617   P., Nenes, A., Onnela, A., Rap, A., Reddington, C. L. S., Riccobono, F., Richards, N. A. D.,
618   Rissanen, M. P., Rondo, L., Sarnela, N., Schobesberger, S., Sengupta, K., Simon, M., Sipilä,
619   M., Smith, J. N., Stozhkov, Y. and Tom, A.: Global particle formation from CERN CLOUD
620   measurements. Science, 354 (6316) 1119-1124, doi:10.1126/science.aaf2649, 2016.

621   Duplissy, J., Merikanto, J., Franchin, A., Tsagkogeorgas, G., Kangasluoma, J., Wimmer, D.,
622   Vuollekoski, H., Schobesberger, S., Lehtipalo, K., Flagan, R. C., Brus, D., Donahue, N. M.,
623   Vehkamäki, H., Almeida, J., Amorim, A., Barmet, P., Bianchi, F., Breitenlechner, M.,
624   Dunne, E. M., Guida, R., Henschel, H., Junninen, H., Kirkby, J., Kürten, A., Kupc, A.,
625   Määttänen, A., Makhmutov, V., Mathot, S., Nieminen, T., Onnela, A., Praplan, A. P.,
626   Riccobono, F., Rondo, L., Steiner, G., Tomé, A., Walther, H., Baltensperger, U., Carslaw, K.
627   S., Dommen, J., Hansel, A., Petäjä, T., Sipilä, M., Stratmann, F., Vrtala, A., Wagner, P. E.,
628   Worsnop, D. R., Curtius, J. and Kulmala, M.: Effect of ions on sulfuric acid-water binary
629   particle formation: 2. Experimental data and comparison with QC-normalized classical
630   nucleation theory, J. Geophys. Res. Atmos., 121 (4), 1752-1775, doi:10.1002/2015JD023538,
631   2016.

632   Ehn, M., Junninen, H., Petäjä, T., Kurtén, T., Kerminen, V.-M., Schobesberger, S.,
633   Manninen, H. E., Ortega, I. K., Vehkamäki, H., Kulmala, M. and Worsnop, D. R.:
634   Composition and temporal behavior of ambient ions in the boreal forest, Atmos. Chem.
635   Phys., 10(17), 8513–8530, doi:10.5194/acp-10-8513-2010, 2010.

636   Ehn, M., Junninen, H., Schobesberger, S., Manninen, H. E., Franchin, A., Sipilä, M., Petäjä,
637   T., Kerminen, V.-M., Tammet, H., Mirme, A., Mirme, S., Hõrrak, U., Kulmala, M. and
638   Worsnop, D. R.: An instrumental comparison of mobility and mass measurements of
639   atmospheric   small   ions,   Aerosol   Sci.   Technol.,   45(4),   522–532,
640   doi:10.1080/02786826.2010.547890, 2011.

641   Ehn, M., Kleist, E., Junninen, H., Petäjä, T., Lönn, G., Schobesberger, S., Dal Maso, M.,
642   Trimborn, A., Kulmala, M., Worsnop, D. R., Wahner, A., Wildt, J. and Mentel, T. F.: Gas
643   phase formation of extremely oxidized pinene reaction products in chamber and ambient air,
644   Atmos. Chem. Phys., 12(11), 5113–5127, doi:10.5194/acp-12-5113-2012, 2012.

645   Ehn, M., Thornton, J. a., Kleist, E., Sipilä, M., Junninen, H., Pullinen, I., Springer, M.,
646   Rubach, F., Tillmann, R., Lee, B., Lopez-Hilfiker, F., Andres, S., Acir, I.-H., Rissanen, M.,
647   Jokinen, T., Schobesberger, S., Kangasluoma, J., Kontkanen, J., Nieminen, T., Kurtén, T.,
648   Nielsen, L. B., Jørgensen, S., Kjaergaard, H. G., Canagaratna, M., Maso, M. D., Berndt, T.,
649   Petäjä, T., Wahner, A., Kerminen, V.-M., Kulmala, M., Worsnop, D. R., Wildt, J. and
650   Mentel, T. F.: A large source of low-volatility secondary organic aerosol, Nature, 506(7489),
651   476–479, doi:10.1038/nature13032, 2014.

652   Franchin, A., Ehrhart, S., Leppä, J., Nieminen, T., Gagné, S., Schobesberger, S., Wimmer,
653   D., Duplissy, J., Riccobono, F., Dunne, E. M., Rondo, L., Downard, A., Bianchi, F., Kupc,
654   A., Tsagkogeorgas, G., Lehtipalo, K., Manninen, H. E., Almeida, J., Amorim, A., Wagner, P.
655   E., Hansel, A., Kirkby, J., Kürrten, A., Donahue, N. M., Makhmutov, V., Mathot, S.,
656   Metzger, A., Petäjä, T., Schnitzhofer, R., Sipilä, M., Stozhkov, Y., Tomé, A., Kerminen, V.
657   M., Carslaw, K., Curtius, J., Baltensperger, U. and Kulmala, M.: Experimental investigation
658   of ion-ion recombination under atmospheric conditions, Atmos. Chem. Phys., 15(13), 7203–
659   7216, doi:10.5194/acp-15-7203-2015, 2015.

660   Hirsikko, A., Nieminen, T., Gagné, S., Lehtipalo, K., Manninen, H. E., Ehn, M., Hõrrak, U.,
661   Kerminen, V.-M., Laakso, L., McMurry, P. H., Mirme, A., Mirme, S., Petäjä, T., Tammet,
662   H., Vakkari, V., Vana, M. and Kulmala, M.: Atmospheric ions and nucleation: a review of
663   observations, Atmos. Chem. Phys., 11(2), 767–798, doi:10.5194/acp-11-767-2011, 2011.

664 Hoyle, C. R., Fuchs, C., Jarvinen, E., Saathoff, H., Dias, A., El Haddad, I., Gysel, M.,
665 Coburn, S. C., Trostl, J., Hansel, A., Bianchi, F., Breitenlechner, M., Corbin, J. C., Craven, J.,
666 Donahue, N. M., Duplissy, J., Ehrhart, S., Frege, C., Gordon, H., Hoppel, N., Heinritzi, M.,
667 Kristensen, T. B., Molteni, U., Nichman, L., Pinterich, T., Prevôt, A. S. H., Simon, M.,
668 Slowik, J. G., Steiner, G., Tome, A., Vogel, A. L., Volkamer, R., Wagner, A. C., Wagner, R.,
669 Wexler, A. S., Williamson, C., Winkler, P. M., Yan, C., Amorim, A., Dommen, J., Curtius,
670 J., Gallagher, M. W., Flagan, R. C., Hansel, A., Kirkby, J., Kulmala, M., Mohler, O.,
671 Stratmann, F., Worsnop, D. R. and Baltensperger, U.: Aqueous phase oxidation of sulphur
672 dioxide by ozone in cloud droplets, Atmos. Chem. Phys., 16(3), 1693–1712, doi:10.5194/acp-
673 16-1693-2016, 2016.

674 Hunter, E. P. and Lias, S. G.: Evaluated gas phase basicities and proton affinity of molecules:
675 an update, J. Phys. Chem. Ref. Data, 27(3), 413–656, 1998.

676 Hyttinen, N., Kupiainen-Määttä, O., Rissanen, M. P., Muuronen, M., Ehn, M. and Kurtén, T.:
677 Modeling the charging of highly oxidized cyclohexene ozonolysis products using nitrate-
678 based   chemical   ionization,   J.   Phys.   Chem.   A,   119(24),   6339–6345,
679 doi:10.1021/acs.jpca.5b01818, 2015.

680 Kirkby, J., Curtius, J., Almeida, J., Dunne, E., Duplissy, J., Ehrhart, S., Franchin, A., Gagné,
681 S., Ickes, L., Kürten, A., Kupc, A., Metzger, A., Riccobono, F., Rondo, L., Schobesberger, S.,
682 Tsagkogeorgas, G., Wimmer, D., Amorim, A., Bianchi, F., Breitenlechner, M., David, A.,
683 Dommen, J., Downard, A., Ehn, M., Flagan, R. C., Haider, S., Hansel, A., Hauser, D., Jud,
684 W., Junninen, H., Kreissl, F., Kvashin, A., Laaksonen, A., Lehtipalo, K., Lima, J., Lovejoy,
685 E. R., Makhmutov, V., Mathot, S., Mikkilä, J., Minginette, P., Mogo, S., Nieminen, T.,
686 Onnela, A., Pereira, P., Petäjä, T., Schnitzhofer, R., Seinfeld, J. H., Sipilä, M., Stozhkov, Y.,
687 Stratmann, F., Tomé, A., Vanhanen, J., Viisanen, Y., Vrtala, A., Wagner, P. E., Walther, H.,
688 Weingartner, E., Wex, H., Winkler, P. M., Carslaw, K. S., Worsnop, D. R., Baltensperger, U.
689 and Kulmala, M.: Role of sulphuric acid, ammonia and galactic cosmic rays in atmospheric
690 aerosol nucleation., Nature, 476(7361), 429–33, doi:10.1038/nature10343, 2011.

691 Kirkby, J., Duplissy, J., Sengupta, K., Frege, C., Gordon, H., Williamson, C., Heinritzi, M.,
692 Simon, M., Yan, C., Almeida, J., Tröstl, J., Nieminen, T., Ortega, I. K., Wagner, R., Adamov,
693 A., Amorim, A., Bernhammer, A.-K., Bianchi, F., Breitenlechner, M., Brilke, S., Chen, X.,
694 Craven, J., Dias, A., Ehrhart, S., Flagan, R. C., Franchin, A., Fuchs, C., Guida, R., Hakala, J.,
695 Hoyle, C. R., Jokinen, T., Junninen, H., Kangasluoma, J., Kim, J., Krapf, M., Kürten, A.,
696 Laaksonen, A., Lehtipalo, K., Makhmutov, V., Mathot, S., Molteni, U., Onnela, A., Peräkylä,
697 O., Piel, F., Petäjä, T., Praplan, A. P., Pringle, K., Rap, A., Richards, N. A. D., Riipinen, I.,
698 Rissanen, M. P., Rondo, L., Sarnela, N., Schobesberger, S., Scott, C. E., Seinfeld, J. H.,
699 Sipilä, M., Steiner, G., Stozhkov, Y., Stratmann, F., Tomé, A., Virtanen, A., Vogel, A. L.,
700 Wagner, A. C., Wagner, P. E., Weingartner, E., Wimmer, D., Winkler, P. M., Ye, P., Zhang,
701 X., Hansel, A., Dommen, J., Donahue, N. M., Worsnop, D. R., Baltensperger, U., Kulmala,
702 M., Carslaw, K. S. and Curtius, J.: Ion-induced nucleation of pure biogenic particles, Nature,
703 533(7604), 521–526, doi:10.1038/nature17953, 2016.

704 Kulmala, M., Vehkamäki, H., Petäjä, T., Dal Maso, M., Lauri, A., Kerminen, V. M., Birmili,
705 W. and McMurry, P. H.: Formation and growth rates of ultrafine atmospheric particles: A
706 review of observations, J. Aerosol Sci., 35(2), 143–176, doi:10.1016/j.jaerosci.2003.10.003,
707 2004.

708 Kürten, A., Bianchi, F., Almeida, J., Kupiainen-Määttä, O., Dunne, E. M., Duplissy, J.,
709 Williamson, C., Barmet, P., Breitenlechner, M., Dommen, J., Donahue, N. M., Flagan, R. C.,
710 Franchin, A., Gordon, H., Hakala, J., Hansel, A., Heinritzi, M., Ickes, L., Jokinen, T.,
711 Kangasluoma, J., Kim, J., Kirkby, J., Kupc, A., Lehtipalo, K., Leiminger, M., Makhmutov,
712 V., Onnela, A., Ortega, I. K., Petäjä, T., Praplan, A. P., Riccobono, F., Rissanen, M. P.,
713 Rondo, L., Schnitzhofer, R., Schobesberger, S., Smith, J. N., Steiner, G., Stozkhov, Y.,
714 Tomé, A., Tröstl, J., Tsagkogeorgas, G., Wagner, P. E., Wimmer, D., Ye, P., Baltensperger,
715 U., Carslaw, K. S., Kulmala, M. and Curtius, J.: Experimental particle formation rates
716 spanning tropospheric sulfuric acid and ammonia abundances, ion production rates, and
717 temperatures, J. Geophys. Res. Atmos., 121, doi:10.1002/2015JD023908, 2016.

718 Lehtipalo, K., Rondo, L., Kontkanen, J., Schobesberger, S., Jokinen, T., Sarnela, N., Kürten,
719 A., Ehrhart, S., Franchin, A., Nieminen, T., Riccobono, F., Sipilä, M., Yli-Juuti, T., Duplissy,
720 J., Adamov, A., Ahlm, L., Almeida, J., Amorim, A., Bianchi, F., Breitenlechner, M.,
721 Dommen, J., Downard, A. J., Dunne, E. M., Flagan, R. C., Guida, R., Hakala, J., Hansel, A.,
722 Jud, W., Kangasluoma, J., Kerminen, V.-M., Keskinen, H., Kim, J., Kirkby, J., Kupc, A.,
723 Kupiainen-Määttä, O., Laaksonen, A., Lawler, M. J., Leiminger, M., Mathot, S., Olenius, T.,
724 Ortega, I. K., Onnela, A., Petäjä, T., Praplan, A. P., Rissanen, M. P., Ruuskanen, T. M.,
725 Santos, F. D., Schallhart, S., Schnitzhofer, R., Simon, M., Smith, J. N., Tröstl, J.,
726 Tsagkogeorgas, G., Tomé, A., Vaattovaara, P., Vehkämäki, H., Vrtala, A. E., Wagner, P. E.,
727 Williamson, C., Wimmer, D., Winkler, P. M., Virtanen, A., Donahue, N. M., Carslaw, K. S.,
728 Baltensperger, U., Riipinen, I., Curtius, J., Worsnop, D. R. and Kulmala, M.: The effect of
729 acid-base clustering and ions on the growth of atmospheric nano-particles, Nat. Commun.,7,
730 doi:10.1038/ncomms11594, 2016.

731 Merikanto, J., Spracklen, D. V, Mann, G. W., Pickering, S. J. and Carslaw, K. S.: Impact of
732 nucleation on global CCN, Atmos. Chem. Phys., 8601–8616, 2009.

733 Merikanto, J., Duplissy, J., Määttänen, A., Henschel, H., Donahue, N. M., Brus, D.,
734 Schobesberger, S., Kulmala, M. and Vehkämäki, H.: Effect of ions on sulfuric acid-water
735 binary particle formation I: Theory for kinetic and nucleation-type particle formation and
736 atmospheric implications, J. Geophys. Res. Atmos., 121, 1736–1751,
737 doi:10.1002/2015JD023538, 2016.

738 Metzger, A., Verheggen, B., Dommen, J., Duplissy, J., Prevot, A. S. H., Weingartner, E.,
739 Riipinen, I., Kulmala, M., Spracklen, D. V, Carslaw, K. S. and Baltensperger, U.: Evidence
740 for the role of organics in aerosol particle formation under atmospheric conditions., Proc.
741 Natl. Acad. Sci. U. S. A., 107(15), 6646–51, doi:10.1073/pnas.0911330107, 2010.

742 Nadykto, A. B.: Uptake of neutral polar vapor molecules by charged clusters/particles:
743 Enhancement due to dipole-charge interaction, J. Geophys. Res. Atmos., 108(D23), 4717,
744 doi:10.1029/2003JD003664, 2003.

745 Ortega, I. K., Kupiainen, O., Kurtén, T., Olenius, T., Wilkman, O., McGrath, M. J.,
746 Loukonen, V. and Vehkämäki, H.: From quantum chemical formation free energies to
747 evaporation rates, Atmos. Chem. Phys., 12(1), 225–235, doi:10.5194/acp-12-225-2012, 2012.

748 Praplan, A. P., Schobesberger, S., Bianchi, F., Rissanen, M. P., Ehn, M., Jokinen, T.,
749 Junninen, H., Adamov, A., Amorim, A., Dommen, J., Duplissy, J., Hakala, J., Hansel, A.,
750 Heinritzi, M., Kangasluoma, J., Kirkby, J., Krapf, M., Kürten, A., Lehtipalo, K., Riccobono,

Atmospheric
Chemistry
and Physics
Discussions

751 F., Rondo, L., Sarnela, N., Simon, M., Tomé, A., Tröstl, J., Winkler, P. M., Williamson, C.,
752 Ye, P., Curtius, J., Baltensperger, U., Donahue, N. M., Kulmala, M. and Worsnop, D. R.:
753 Elemental composition and clustering behaviour of α-pinene oxidation products for different
754 oxidation conditions, Atmos. Chem. Phys., 15(8), 4145–4159, doi:10.5194/acp-15-4145-
755 2015, 2015.

756 Riccobono, F., Schobesberger, S., Scott, C. E., Dommen, J., Ortega, I. K., Rondo, L.,
757 Almeida, J., Amorim, A., Bianchi, F., Breitenlechner, M., David, A., Downard, A., Dunne, E.
758 M., Duplissy, J., Ehrhart, S., Flagan, R. C., Franchin, A., Hansel, A., Junninen, H., Kajos, M.,
759 Keskinen, H., Kupc, A., Kürten, A., Kvashin, A. N., Laaksonen, A., Lehtipalo, K.,
760 Makhmutov, V., Mathot, S., Nieminen, T., Onnela, A., Petäjä, T., Praplan, A. P., Santos, F.
761 D., Schallhart, S., Seinfeld, J. H., Sipilä, M., Spracklen, D. V, Stozhkov, Y., Stratmann, F.,
762 Tomé, A., Tsagkogeorgas, G., Vaattovaara, P., Viisanen, Y., Vrtala, A., Wagner, P. E.,
763 Donahue, N. M., Kirkby, J., Kulmala, M., Worsnop, D. R. and Baltensperger, U.: Oxidation
764 products of biogenic emissions contribute to nucleation of atmospheric particles, Science,
765 344, 717–721,doi:10.1126/science.1243527, 2014.

766 Rissanen, M. P., Kurtén, T., Sipilä, M., Thornton, J. A., Kausiala, O., Garmash, O.,
767 Kjaergaard, H. G., Petäjä, T., Worsnop, D. R., Ehn, M. and Kulmala, M.: Effects of chemical
768 complexity on the autoxidation mechanisms of endocyclic alkene ozonolysis products: From
769 methylcyclohexenes toward understanding α-pinene, J. Phys. Chem. A, 119(19), 4633–4650,
770 doi:10.1021/jp510966g, 2015.

771 Schobesberger, S., Junninen, H., Bianchi, F., Lönn, G., Ehn, M., Lehtipalo, K., Dommen, J.,
772 Ehrhart, S., Ortega, I. K., Franchin, A., Nieminen, T., Riccobono, F., Hutterli, M., Duplissy,
773 J., Almeida, J., Amorim, A., Breitenlechner, M., Downard, A. J., Dunne, E. M., Flagan, R.
774 C., Kajos, M., Keskinen, H., Kirkby, J., Kupc, A., Kürten, A., Kurtén, T., Laaksonen, A.,
775 Mathot, S., Onnela, A., Praplan, A. P., Rondo, L., Santos, F. D., Schallhart, S., Schnitzhofer,
776 R., Sipilä, M., Tomé, A., Tsagkogeorgas, G., Vehkamäki, H., Wimmer, D., Baltensperger, U.,
777 Carslaw, K. S., Curtius, J., Hansel, A., Petäjä, T., Kulmala, M., Donahue, N. M. and
778 Worsnop, D. R.: Molecular understanding of atmospheric particle formation from sulfuric
779 acid and large oxidized organic molecules., Proc. Natl. Acad. Sci. U. S. A., 110(43), 17223–
780 8, doi:10.1073/pnas.1306973110, 2013.

781 Shuman, N. S., Hunton, D. E. and Viggiano, A. A.: Ambient and modified atmospheric ion
782 chemistry: from top to bottom, Chem. Rev., 115(10), 4542–4570, doi:10.1021/cr5003479,
783 2015.

784 Steiner, G., Jokinen, T., Junninen, H., Sipilä, M., Petäjä, T., Worsnop, D., Reischl, G. P. and
785 Kulmala, M.: High-resolution mobility and mass spectrometry of negative ions produced in a
786 241 Am aerosol charger, Aerosol Sci. Technol., 48 (3), 261–270,
787 doi:10.1080/02786826.2013.870327, 2014.

788 Tröstl, J., Chuang, W. K., Gordon, H., Heinritzi, M., Yan, C., Molteni, U., Ahlm, L., Frege,
789 C., Bianchi, F., Wagner, R., Simon, M., Lehtipalo, K., Williamson, C., Craven, J. S.,
790 Duplissy, J., Adamov, A., Almeida, J., Bernhammer, A.-K., Breitenlechner, M., Brilke, S.,
791 Dias, A., Ehrhart, S., Flagan, R. C., Franchin, A., Fuchs, C., Guida, R., Gysel, M., Hansel, A.,
792 Hoyle, C. R., Jokinen, T., Junninen, H., Kangasluoma, J., Keskinen, H., Kim, J., Krapf, M.,
793 Kürten, A., Laaksonen, A., Lawler, M. J., Leiminger, M., Mathot, S., Möhler, O., Nieminen,
794 T., Onnela, A., Petäjä, T., Piel, F., Miettinen, P., Rissanen, M. P., Rondo, L., Sarnela, N.,

Atmospheric
Chemistry
and Physics
Discussions

Open Access

EGU

795   Schobesberger, S., Sengupta, K., Sipilä, M., Smith, J. N., Steiner, G., Tomé, A., Virtanen, A.,
796   Wagner, A. C., Weingartner, E., Wimmer, D., Winkler, P. M., Ye, P., Carslaw, K. S.,
797   Curtius, J., Dommen, J., Kirkby, J., Kulmala, M., Riipinen, I., Worsnop, D. R., Donahue, N.
798   M. and Baltensperger, U.: The role of low-volatility organic compounds for initial particle
799   growth in the atmosphere, Nature, 533, 527–531, doi:doi:10.1038/nature18271, 2016.

800   Zhao, Y. and Truhlar, D. G.: The M06 suite of density functionals for main group
801   thermochemistry, thermochemical kinetics, noncovalent interactions, excited states, and
802   transition elements: Two new functionals and systematic testing of four M06-class
803   functionals and 12 other functionals, Theor. Chem. Acc., 120(1–3), 215–241,
804   doi:10.1007/s00214-007-0310-x, 2008.

805